A PRELIMINARY INVESTIGATION OF COLD GAS INJECTION INTO A FORWARD-FACING CAVITY IN HYPERSONIC FLOW

Sidra I. Silton* **and David B. Goldstein†**
Center for Aeromechanics Research
Department of Aerospace Engineering & Engineering Mechanics
The University of Texas at Austin
Austin, TX 78712-1085

Abstract

Hypersonic flow over the nose of a blunt body with a forward-facing cavity into which cold gas is injected is examined. Numerical calculations indicate that bow shock oscillations remain the same or increase in amplitude and frequency compared to a cavity with no mass injection depending on the direction of injection (radial or axial) and the gas injected (air or helium). Strong resonant pressure oscillations which occur within the cavity draw the injected gas out of the cavity during the outflow portion of the cycle and cause the injected gas to pool in the cavity during inflow. The injected gas remains cold even after exiting the cavity.

1 Introduction

Hypersonic vehicles are designed to withstand severe heat loads. Maximum heating and, hence, the potential for material ablation, is typically most critical at the nose tip. Recently, several papers have appeared involving the use of a forward facing cavity in the nose tip to reduce stagnation point heating.

Preliminary experiments using an infrared (IR) camera by Yuceil et al. [1] indicated that larger diameter, shallow cavities (length-to-diameter (L/D) between 0.15 and 0.35) created a stable 'cool ring' just outside of a sharp cavity lip with temperatures locally lower than those found on a simple spherical nose. A joint numerical and experimental study by Engblom et al. [2] concluded that sharp cavity lips produce not only a separated recirculation region (accounting for the 'cool ring') but also severe heating just inside the cavity for weakly oscillating flows. In time-accurate numerical simulations by Engblom et al. [3], it was found that resonant oscillations are obtained if either freestream fluctuations are present or a sufficiently deep cavity is employed.

Yuceil [4] reported experimental results for a deep cavity with an L/D=2.0 for which he found substantial cooling over the entire nose region compared to the baseline case (no cavity). Engblom and Goldstein [5] showed that substantial surface nose-tip cooling is achieved by creating strong longitudinal pressure oscillations within the cavity to induce large bow shock oscillations. That numerical effort also found that the heat reduction benefit appeared to increase with mean relative bow shock speed.

In order to control the shock oscillations, mass injection has been explored. Marquart et al. [6] found experimentally that low flow rate mass injection through four radial jets into a cavity reduced the amplitude of shock oscillations inside that cavity. For a freestream Mach number of 10, Huebner and Utreja [7] also observed an increase in shock stability (i.e. decrease in shock oscillation strength) for their half-scale deep cavity case with radial mass injection through four ports lying $\pm 45°$ from the axis of symmetry. Johnson [8], however, found that a flow instability was observed when a small quantity of gas was injected forward along the axis of symmetry into the back of the cavity (referred to hereafter as axial mass injection) under freestream conditions of M=22. Johnson suggests that the mechanism causing this instability involves the successive formation and shedding of non-axisymmetric vortices inside the cavity.

The possible mechanisms by which mass injection could damp bow shock oscillations remains uncertain. It could be that the injected material disrupts the axially moving waves and increases dissipation. That is, the injected material may produce severe temperature fluctuations in the cavity which diffract strong waves. As to increasing oscillation strength for axial jets, besides Johnson's suggestion, there may be other possibilities as yet undetermined.

The objective of this study is to investigate the effects of cold gas injection on a forward-facing cavity's oscillating shock dynamics. The results also shed some light on the possible uses of mass injection in various supersonic combustor geometries.

This paper presents results from a numerical study of the fluid mechanics and basic thermodynamics (heating rates are not specifically sought after) of forward-facing cavity flows with either axial or radial

*Graduate Research Assistant, Student Member AIAA
†Assistant Professor, Member AIAA

Copyright © 1997 by the American Institute of Aeronautics and Astronautics, Inc. All rights reserved.

mass injection. We first discuss the computational modeling used with particular emphasis on grid resolution requirements in Section 2. The first set of results presented in section 3.1 includes numerical simulation data for an axial mass injector using both air and helium. Section 3.2 provides results for a radial helium mass injector.

2 Methodology

2.1 Computer Code Description

A commercial computer code, INCA (licensed from Amtec Engineering), was used for this study. INCA is a finite-volume code which utilizes flux splitting with upwinding to capture strong shocks. Fluxes are computed with the flux splitting of Steger and Warming. INCA offers an efficient Lower-Upper Successive Gauss-Seidel (LU-SGS) implicit solver to calculate steady flowfields. The LU-SGS algorithm approximately solves the system of equations using two sweeps of a point Gauss-Seidel relaxation. INCA offers a variation of the LU-SGS implicit solver to calculate unsteady flows which was utilized in the present work. This algorithm permits much larger time steps than a simple Euler step method by performing a sufficient number of sub-iterations at each time step. This algorithm is also second-order accurate in time.

INCA allows for the addition of multiple species through the specification of the species type, the species molecular weight, and Blottner's viscosity coefficients. Blottner's viscosity coefficients are also used to calculate the thermal conductivity for each species using the Eucken-Wilkes method. Specification of the Schmidt Number and the coefficients for the temperature dependent curves for the calculation of specific heat, enthalpy, and entropy, for each species is also required. This program also allows for the addition of the two equation k-ϵ turbulence model.

All grid generation is performed using an algebraic grid generation code which is capable of producing near orthogonal grids based and utilizes exponential-linear-exponential spacing.

2.2 Numerical Assumptions

A hemispherically blunted cylinder, 5.08 cm in diameter, with an axial cavity of length L from the base to the lip (Fig. 1) is modeled. The cavity diameter (D) is 2.54 cm. The length of the cavity is 5.08 cm, giving a length to diameter ratio of 2.0. The cavity lip is modeled as sharp. This geometry at Mach 5 has been

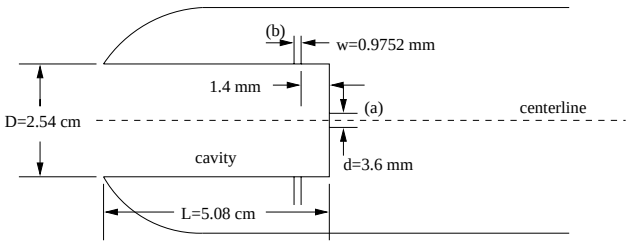

Figure 1: Schematic of axial cavity in the nose region of a hypersonic vehicle.(a) Indicates position of axial jet. (b) Indicates position of radial slot jet.

determined by Engblom and Goldstein [5] to undergo self-sustaining shock wave oscillations.

For modeling mass injection, the exit plane of a supersonic nozzle is introduced into the model on one portion of the cavity surface. For axial mass injection, the radius of the exit plane was 1.8 mm with the jet centerline on the axis of symmetry (indicated by (a) in fig. 1). For radial mass injection, the width of the exit plane was 0.9752 mm and the jet circumscribed the entire perimeter of the cavity at a distance of 1.41 mm from the base of the cavity (indicated by (b) in fig. 1). At the injector inflow plane, velocity, temperature, and pressure were specified as constants.

The freestream gas was air of Mach number 5. The air temperature and pressure were specified as 64 K and 4.7 kPa, respectively. Air or helium was used as the gas for the mass injection into the cavity. We may define a dimensionless mass flow coefficient

$$\dot{m}_c \equiv \frac{\dot{m}_{jet}}{\dot{m}_{cavity}} \tag{1}$$

where $\dot{m}_{cavity}$ is the mass flow due to freestream conditions into the projected cavity mouth and $\dot{m}_{jet}$ is the mass injection flow rate. Axial air mass injection had $\dot{m}_c$=0.0769 at an injector Mach number of 1.005, a temperature of 60 K, and a pressure of 85 kPa at the exit plane. For axial helium mass injection, $\dot{m}_c$=0.0313 was used at an injector Mach number of 1.01, and the same static temperature and pressure at the exit plane. For the radial helium mass injection, $\dot{m}_c$=0.240. All other exit plane run parameters for radial helium mass injection were specified at the same values as in the axial helium mass injection case. These and other specific run parameters are summarized in table 1.

Several simplifying assumptions were made in the simulations. First, the wall temperature was assumed

Gas	air	helium	
γ	1.4	1.66	
R (J/kg K)	287	2076	
Pressure (kPa)	85	85	
Temperature (K)	60	60	
$\mu(Pa \cdot sec)$	1.0×10^{-5}	6.46×10^{-6}	
Mach Number	1.005	1.01	
injection type*	axial	axial	radial
jet size (mm)	1.8	1.8	0.9752
$\dot{m}_c$	$7.7x10^{-2}$	$3.1x10^{-2}$	$2.4x10^{-1}$
$Re_{injector}$	$2.8x10^5$	$1.8x10^5$	$4.7x10^4$

Table 1: Exit plane run parameters for injected gas

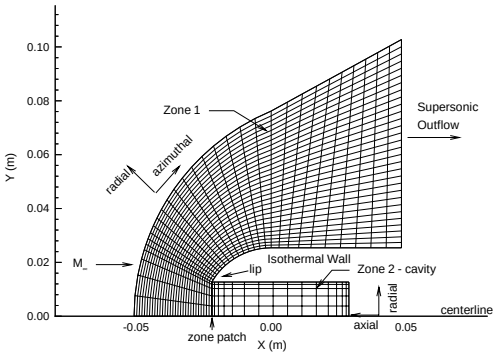

Figure 2: Schematic two zone grid as used for numerical calculations.

isothermal (T_{wall}=300 K). As a reasonable approximation, both the air and helium were assumed calorically perfect. Also, the flow was assumed axisymmetric. This was appropriate because pressure oscillations at the cavity base in the deep cavity experiments of Yuceil [4] are typically planar (i.e., negligible radial variations) when there is no mass injection. Axisymmetric mass injection was assumed not to produce appreciable non-axisymmetric flow. Due to the small scale of the flowfield (i.e., nose region), laminar flow is assumed for the axial injection case and initially for the radial injection case. The freestream Reynolds number based on body diameter was roughly 5.0x10^5 cm^{-1}. The actual Reynolds number per centimeter was much smaller along the body surface inside the cavity and outside the cavity near the lip due to the low speed of the flow. Since the characteristic flow lengths were less than one centimeter and a favorable pressure gradient was often present, transition to turbulent flow might not be expected to occur within the cavity unless the oscillation and gas injection within the cavity cause the flow to 'trip'. For the jet configurations in the present work, however, the maximum $Re_{injector}$ is 2.8x10^5 and the laminar flow assumptions for the cavity with injection were thus doubtful in practice as will be shown in section 2.3. Hence, we place greater emphasis on utilizing a turbulence model described below.

2.3 Numerical Procedure

A surface cell thickness of 1.0E-4 m was chosen to obtain a relatively fine grid near the body surface since heat transfer rates were not a concern for the present work. This cell thickness and the initial (coarse) grid were determined by reviewing the grid refinement studies of Engblom et al. [2]. A two-zone grid, in which one zone contains only the cavity region was implemented (fig. 2). The shock does occasionally cross the boundary between the two zones when air was injected, but results show that this had a negligible effect on accuracy.

A grid refinement study was conducted for the axial injection case to determine if the interior cell resolution was fine enough to capture the mass diffusion between helium and air. This study found that a fine mesh with twice the number of grid points in the axial, azimuthal, and radial directions in both zones produced a more distinct concentration contour boundaries between the helium and air. However, the same vortex ring patterns were apparent after two to three cycles and the overall contour patterns of species concentrations were the same. This grid refinement study also found that the pressure contours and the base pressure history plots showed the same trends for both runs. Due to these similarities in the fluid dynamic trends, it was decided that for the present work the coarse grid (zone 1 - 80x120, zone 2 - 30x90) produced acceptable results and further Direct Numerical Simulation (DNS) used this grid.

A second grid refinement study was conducted for the radial injection case. This was done because the initial investigation of the radial case showed the vortex dynamics to be more complicated than those found in the axial injection case. It was found that finer meshes produced significantly different trends in the vortex dynamics when DNS without any turbulence model was attempted. These differences included an increase in the number of vortices with finer meshes (the coarse mesh produced almost no vortices at all)

*For radial injection, jet size is the width of the jet, and $Re_{injector}$ is based on width of jet. For axial injection, jet size is the radius of the jet and $Re_{injector}$ is based on the diameter of the jet.

as well as variations in vortex positions in the cavity, different rates of diffusion rates between the helium and air as indicated by different concentration contours, and somewhat chaotic behavior of the cavity pressure contours and base pressure trace. Figure 3 is representative of the complicated nature of the flow in the cavity for DNS. Because the differences did not disappear as progressively finer meshes were used (doubled in radial direction, tripled in the axial direction, then doubled again in the radial direction and increased 50% in the axial direction), it seemed unlikely that grid convergence would be obtained using the available computational resources. For this reason, a two equation k-ϵ turbulence model was utilized and the grid convergence study was repeated.

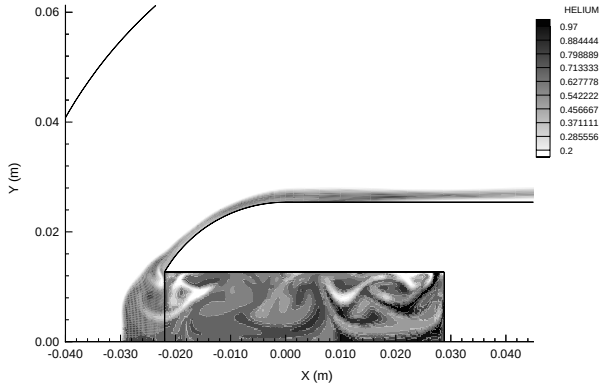

Figure 3: Helium contours for the radial injection DNS case.

With the turbulence model on, the first two computational cycles (startup) of a coarse resolution (zone 1 - 80x120, zone 2 - 30x90), medium resolution (zone 1 - 110x120, zone 2 - 60x270), and fine resolution (zone 1 - 170x120, zone 2 - 120x360) grids were compared. Prior to the first cycle, the flowfield started as two distinct regions: within the cavity, the air was at rest at stagnation point conditions, while everywhere else, the air was moving at freestream conditions. During the dramatic motion of the first two cycles, the position of the bow shock was established and some of the later fluid dynamic trends were seen. During startup, the coarse grid run had smoother helium contours than the medium grid. Interspecies diffusion appeared more rapid on the coarse grid. However, there were no substantial changes between a medium and fine resolution grid (i.e. helium concentration and pressure contours were practically identical). Hence, grid convergence was assumed to occur at the medium grid level. To demonstrate this convergence, concentration contours on the medium and fine resolution grids were compared in figure 4 after a third computational cycle at the same point in the cycle (i.e. point of lowest base pressure). The medium resolution grid with the k-ϵ turbulence model was thus utilized to obtain the results for the radial gas injection case.

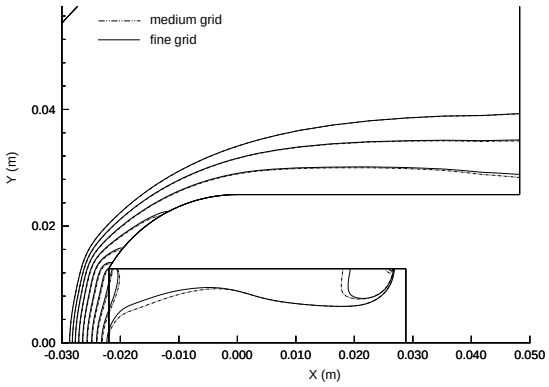

Figure 4: Comparison of 10 helium concentration contours showing grid convergence between medium and fine resolution grids.

To examine the temporal convergence, time-accurate simulations were conducted for the case of radial helium injection into the cavity using a steady oscillating flow field solution as an initial condition. This case was chosen because it appeared to have the finest flow scales of the three cases that were investigated. The sensitivity of the residual (the measure of global convergence level) and the base pressure history trace to the global time step and number of sub-iterations was studied for representative cases with the turbulence model off. A three to four order of magnitude change in the residual per time step was desired while trends in the base pressure history traces must be the same. This study ensured temporal convergence and helped to determine which parameters provide the most efficient solution (minimum cost). Then, with the turbulence model turned on, the time step was further reduced to again verify temporal convergence. Generally, one pressure oscillation cycle was solved using approximately 4,000 global time steps (depending on oscillation frequency) with 6 sub-iterations per time step. The corresponding CPU time requirement was typically 20-38 hours/cycle on a DEC Alpha 3000/700 depending on the options utilized.

The results for the axial mass injection were obtained using time-accurate simulations with a steady oscillating flow field solution as an initial condition. The results for the radial helium injection were ob-

tained using time-accurate simulations beginning from startup (as described above) with the k-ϵ turbulence model.

3 Results

The device modeled resembles the model used in the Mach 5 tests conducted at The University of Texas at Austin [2]. Upstream of a L/D=2.0 cavity, the shock undergoes self-sustaining oscillations. Computational results for a shock undergoing self-sustaining oscillations with no mass injection are discussed by Engblom and Goldstein [5].

3.1 Axial Mass Injection

When a cold gas is introduced into the cavity along its centerline, the magnitude of the shock oscillations is greater than the case of no mass injection. The shock oscillation does not appear to be damped by the mass injection as was initially expected base on the works of Marquart et al. [6] and Huebner and Utreja [7]. However, the fluid mechanisms associated with the oscillations are different. The observed increase in bow shock oscillation strength is most likely related to the increased instability observed by Johnson [8].

3.1.1 Air Injection

The shock oscillation with axial air injection appears to be larger than in the baseline case with no gas injection. The cold stream of air forces the shock to move a greater distance away from the lip of the cavity (fig. 5) than in the no injection case during the outflow portion of the cycle. The cold air stream is dragged out of the cavity during this portion of the cycle by the co-flowing exhausting cavity gas and impinges on the lip as the flow is turned back toward the body by the high pressure region just downstream of the bow shock. The cold air remains close to the body and relatively cool as indicated by area 1 of figure 6. During the inflow portion of the cycle, the shock approaches closer to the lip of the cavity (fig. 7) as compared to the no injection case. The cold air that has not been blown clear is pushed back into the cavity, but does not fill the cavity. The frequency of oscillation (1456 Hz) is roughly the same as in the no injection case (1500 Hz)[9]. The difference in the frequency of oscillation should be due to the somewhat greater bow shock standoff distance, L^*, the distance between the mean bow shock location and the cavity base along the centerline, since the overall distance traveled by the bow shock when cold air is injected is slightly greater

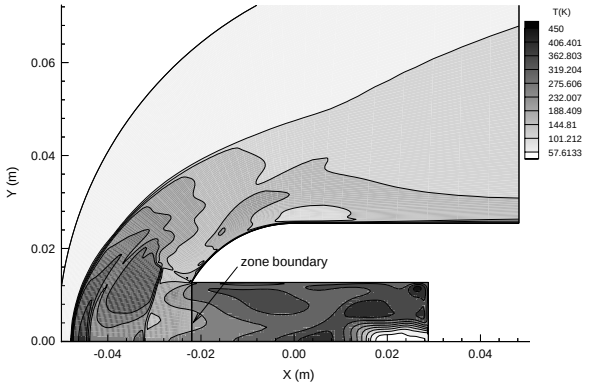

Figure 5: Temperature contours of outflow portion of cycle during cold axial air injection. Shock at position farthest from cavity lip (most forward position).

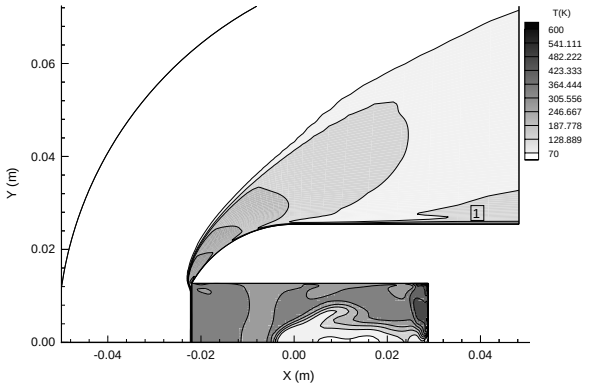

Figure 6: Cold axially injected air remains close to body after exiting cavity as indicated by the (1) in these temperature contours.

than that without air injection. The difference in the frequency may also be due to a slower speed of sound since the mean temperature within the cavity dropped due to the injection of cold air.

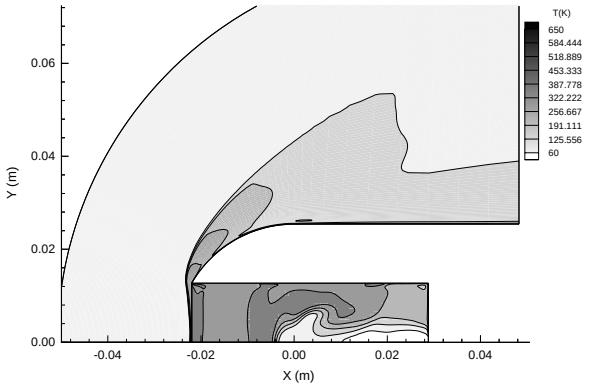

Figure 7: Temperature contours of the inflow portion of cycle during cold axial air injection. Shock at position closest to the cavity lip.

The pressure oscillations within the cavity vary from one half an atmosphere to three atmospheres during the course of a cycle. The highest pressure occurs outside of the cavity, behind the shock as it begins to move forward during the outflow portion of the cycle (fig. 8). It is possible that this large pressure variation is a contributing factor to the the maximum bow shock standoff distance being as large as was observed and that the oscillation strength of the bow shock (instability of the flow) was increased as seen by Johnson [8], although the phenomena observed by Johnson was not axisymmetric and this numerical study, by definition, is axisymmetric. Another possibility for the increase in bow shock oscillation strength is that the air injection with pressure wave induced jet pinch-off is acting as a periodic forcing function if a spring-mass-damper model similar to that discussed by Engblom [9] holds true in this case.

3.1.2 Helium Injection

Helium has a much lower molecular weight than air, and thus has a higher sonic velocity than air at a given temperature. The higher sonic velocity is believed to cause an increase in the oscillation frequency of the bow shock when helium is injected into the cavity (1800 Hz) over that of the bow shock when no mass is injected (1500 Hz) [9]. The oscillation frequency, f_1, is expected to follow from the primary mode frequency calculated from equation 1 of reference [2], here rewritten as

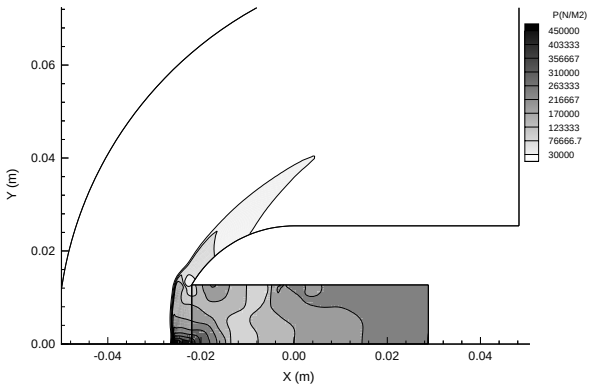

Figure 8: Snapshot in time of highest pressure level occurrence during a cycle of the cold axial air injection.

$$f_1 = \frac{\bar{a}}{4L^*} \tag{2}$$

where here

$$\bar{a} = \frac{1}{2}(a_{stag} + a_{He}) \tag{3}$$

is roughly the average speed of sound between the bow shock and the cavity basewall. The speed of sound, a, is defined as

$$a = \sqrt{\gamma RT} \tag{4}$$

where γ is the ratio of the specific heats, R is the gas constant and T is the temperature of the stagnant gas in the cavity, T_{stag} when calculating a_{stag}. When calculating a_{He}, T is the stagnation temperature of the cold gas injected, $T_{stag,He}$. Obviously, depending on the actual fluid dynamics, the mean speed of sound along L^* may vary from $\bar{a}$.

The discrepancy in the oscillation frequency (1800 Hz vs. 1500 Hz) can be explained using equation 2. The speed of sound for the helium injection is approximately 498 m/sec which leads to a mean cavity speed of sound of 424 m/sec from equation 3, as compared to 350 m/sec in the no-gas-injection baseline case. Assuming that the distance between the mean bow shock location and the cavity base along the centerline is approximately constant between the two cases, equation 2 predicts an oscillation frequency of 1496 Hz for the case with no mass injection and 1812 Hz for the helium injection case. The agreement between the observed and calculated frequencies for the case of axial helium injection seems good.

The helium spreads within the cavity during the inflow portion of the shock oscillation cycle (as the shock moves towards the cavity mouth), but fails to fill the cavity (fig. 9). As the pressure wave during

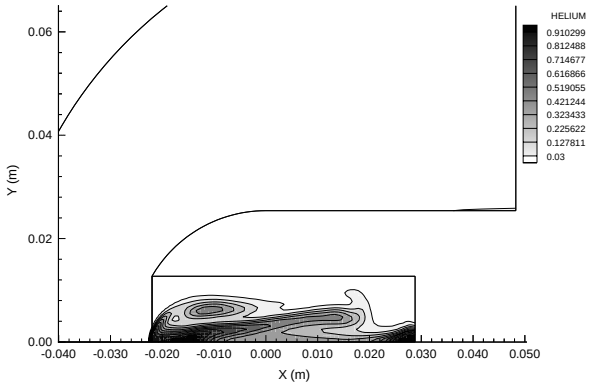

Figure 9: Helium concentration contours of the inflow portion of axial injection case. Helium remains within the cavity, but fails to fill it.

inflow reaches the back of the cavity, it appears to constrict the jet. The pressure wave reflected off the cavity basewall is then followed forward by a strong vortex ring whose core is filled with helium. The ring is then dragged out of the cavity as the shock moves far enough upstream from the cavity lip to allow the vortex ring of helium to be caught up in the mean outflowing streamlines (fig. 10). These streamlines force

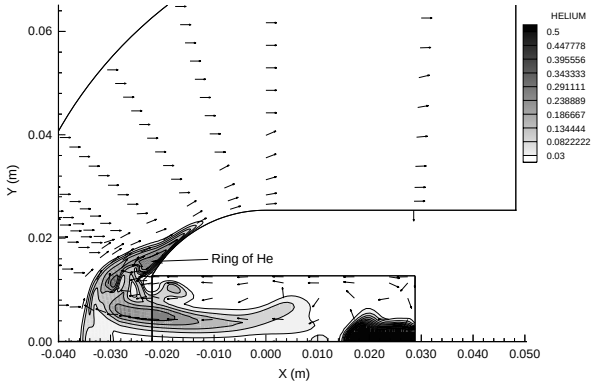

Figure 10: Helium concentration contours of the outflow portion of axial injection case with overlaid velocity vectors. Velocity vectors show direction of flow only.

the rings of helium back towards the body. Once outside the cavity, the helium remains close to the body wall. Each helium ring moving around the body experiences an axisymmetric stretching. These areas of high helium concentration diffuse into the air once they are outside of the cavity and remain cool (fig. 11b).

The diffusion may be hindered by the rapid rotation of the stretched vortex cores and the centrifugal species separation effect. Figures 11a and 11b show that the helium remains cold throughout the entire cycle until the helium becomes diffused into the air. This interaction mechanism appears novel.

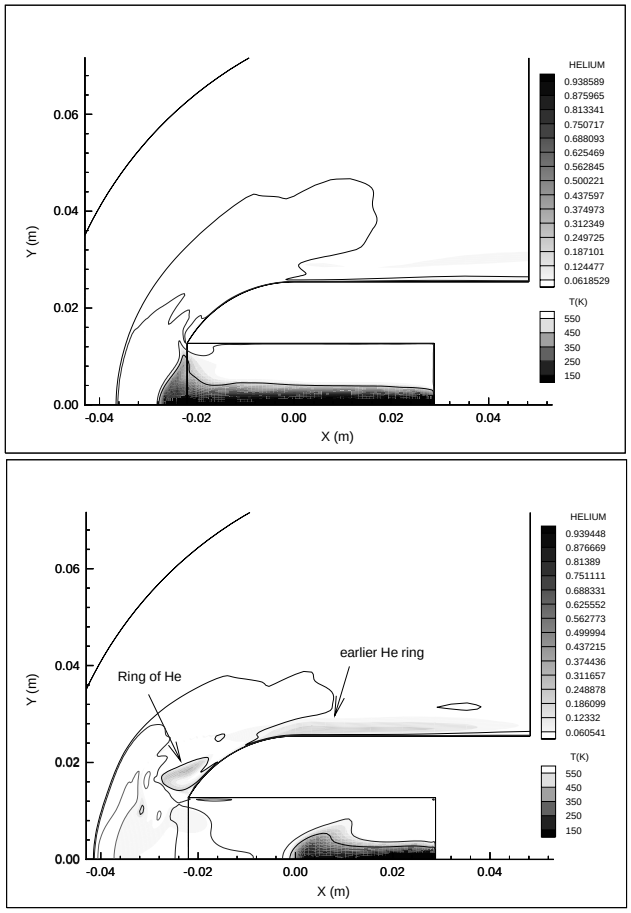

Figure 11: Temperature line contours overlaid on concentration contours to show heating trends of helium throughout cycle for axial helium injection case. (a) top - mid-cycle, all helium remains cool. (b) bottom - helium diffusing into air outside of cavity in rings begins to warm.

The variations in pressure are not as great with helium injection as with air injection. In the case of helium injection the highest pressure oscillations appear to be confined to the bottom half of the cavity. A small area of high pressure also occurs behind the bow shock just before it begins to move forward (fig. 12). This high pressure spot does not appear to be as large in size or strength as that seen in the axial air injection. This may contribute to the slightly weaker shock oscillation for the axial helium injection over that of

the air injection. The distance the bow shock travels, however, is still greater than that of the no injection case and is a partial explanation for the difference in calculated and observed frequency mentioned above.

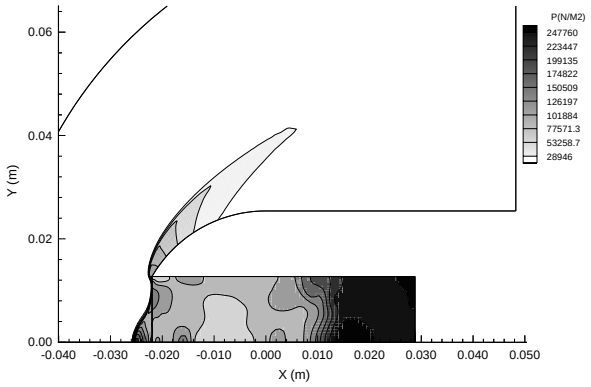

Figure 12: Pressure contour plot for axial helium injection case just prior to the bow show beginning to move forward.

3.2 Radial Helium Injection

Now consider the separate case of radial helium gas injection. In this case, the injected gas has no forward momentum with which to create a strong forward moving jet. Yet the shock oscillations during radial mass injection are comparable to those without mass injection, approaching a steady level after perhaps ten cycles (fig. 13). Although a completely steady-state oscillation is not reached, the solution is believed to be asymptotically approaching a steady-state limit. As in the case of axial helium injection, the frequency of oscillation (approximately 1925 Hz) increased over the case of no mass injection (1496 Hz). The increase in oscillation frequency of the radial helium injection over that of the axial helium injection is most likely due to the cavity now being nearly fully filled with helium.

This study of radial helium injection shows that even large amounts of mass injection is not enough to decrease the bow shock oscillation as was believed by Marquart et al. [6] and Huebner and Utreja [7]. However, the parameters used for the present numerical study are sufficiently different from those used in [6] and [7] that complete agreement could not be expected. Considering the uniformity of the helium within the cavity and the smoothness of the oscillations, it would appear that the same mechanisms are responsible for self-sustained oscillations as were discussed by Engblom [9] for a cavity without mass injection.

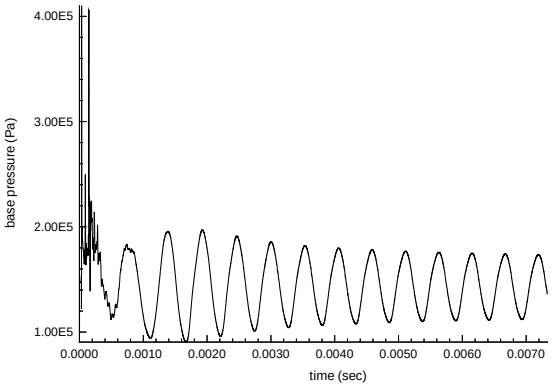

Figure 13: Base pressure history plot for radial helium injection from startup.

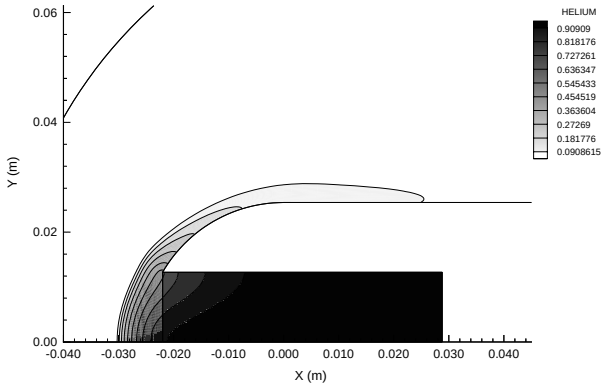

Figure 14: Helium concentration contours for radial injection showing helium just beginning to escape from the cavity.

During the inflow portion of the first cycle, the helium completely fills the cavity, and the cavity remains filled with high concentrations of helium from that time on. On the outflow portion of each following cycle (fig. 14), helium flows out of the cavity in cool streams which represent turbulence model smoothed vortex cores. These areas of helium continue to diffuse into the air once they are outside of the cavity and moving downstream, creating a cool helium film over the body (fig. 15). The cool helium being convected around the body is believed to increase the cooling effect during outflow since it protects the body surface as the movement of the shock increases the relative Mach number and therefore the temperature of the nearby gas. During the inflow portion of the cycle, the helium

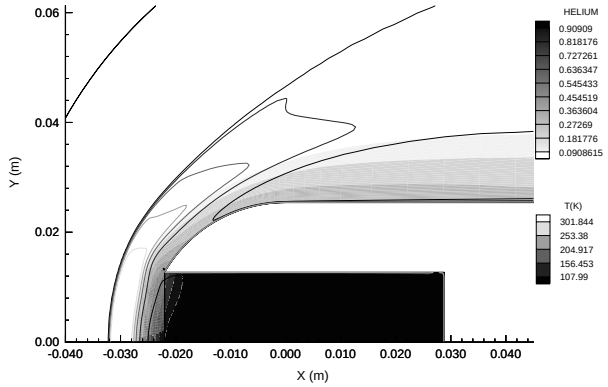

Figure 15: Temperature contours overlaid on helium concentration contours for radial injection with the shock moving aft of helium film forming around body.

that has not flowed out of the cavity is pushed back into the cavity by the high pressure air behind the approaching bow shock and remains in the cavity (fig. 16) until the shock begins to move forward again.

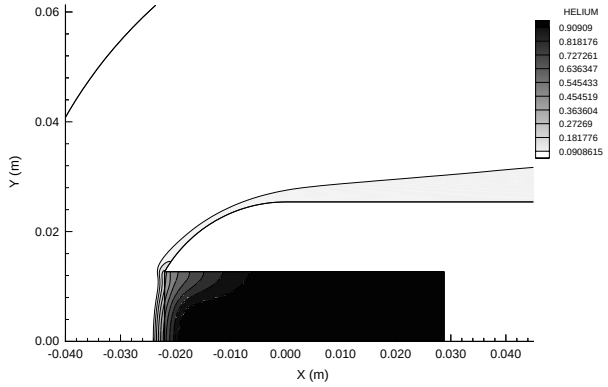

Figure 16: Helium concentration contours for radial injection of helium being restricted to cavity when shock approaches cavity lip.

The pressure waves within the cavity remain relatively planar for this case (fig. 17) which may in part account for the sinusoidal appearance of the base pressure history (fig. 13) and in turn the steady bow shock oscillations.

Discussion

Shock oscillations due to pressure waves inside a forward-facing cavity are altered by mass injection into the cavity. Axial cold air injection increases the magnitude of the shock oscillation while having almost no effect on the bow shock oscillation frequency. The injected air remains cold after exiting the cavity and is likely to increase the cooling on the cavity lip. Cold helium injection, however, causes the frequency of the shock oscillations to increase over that with no mass injection most likely due to the high speed of sound of the helium. Axial helium injection is also found to cause the distance which the shock oscillations cover to increase, while the radial helium injection produces little change in magnitude of the shock oscillations. The helium remains cold and diffuses little once outside the cavity in both cases. Radially injected helium flows out of the cavity periodically in cold streams. The mechanism which causes the periodic outflow of He from the cavity could be used as a flow control valve for a fuel (e.g. H_2) which would remain cold until it was otherwise required by a downstream combustor. That is, the ability to inject, say, H_2 into a hypersonic freestream while keeping it cool and retarding mixing is interesting. If the gas is found not to move far enough away to prove useful for fuel injection, the coincident possibility of using the ejected cold gas to film cool the injector structure may prove useful.

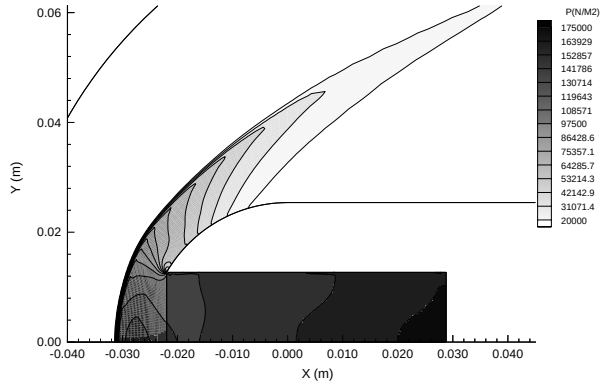

Figure 17: Pressure contours for radial helium injection case are relatively planar.

Acknowledgments

The authors are grateful to Dr. William Engblom for many helpful technical discussions.

References

[1] Yuceil, B., Dolling, D.S., and Wilson, D., "A Preliminary Investigation of the Helmholtz Resonator Concept for Heat Flux Reduction", AIAA Paper 93-2742, July 1993.

[2] Engblom, W.A., Yuceil, B., Goldstein, D.B., and

Dolling, D.S., "Experimental and Numerical Study of Hypersonic Forward-Facing Flow," *Journal of Spacecraft and Rocket*, Volume 33, No. 3, May-June 1996, pp.353-359.

[3] Engblom, W.A., Goldstein, D.B., Ladoon, D., and Schneider, S., "Fluid Dynamics of Forward-Facing Cavity Flow," AIAA Paper 96-0667, Jan. 1996.

[4] Yuceil, B., "An Experimental Investigation of a Forward-Facing Nose Cavity on a Blunt Body at Mach 5," The University of Texas at Austin Ph.D. Dissertation, Dec. 1995, pp. 77- 94.

[5] Engblom, W.A. and Goldstein, D.B., "Nose-Tip Surface Heat Reduction Mechanism," AIAA Paper 96-0354, Jan. 1996.

[6] Marquart, E.J., Grubb, J.P., and Utreja, L., "Bow Shock Dynamics of a Forward Facing Nose Cavity," AIAA Paper 87-2709, Oct. 1987.

[7] Huebner, L. E. and Utreja, L. R., "Experimental Flowfield Measurement of a Nose Cavity Configuration," SAE, Aerospace Technology Conference and Exposition, Long Beach, CA, October 5-8, 1987.

[8] Johnson, R. H., "Instability in Hypersonic Flow about Blunt Bodies," *The Physics of Fluids*, Volume 2, No. 5, Sept-Oct. 1959, pp. 526-532.

[9] Engblom, W.A., "Numerical Investigation of Hypersonic Flow Over a Forward-Facing Cavity," The University of Texas at Austin Ph.D. Dissertation, August 1996.